Chemical vapor infiltration of SiC with microwave heating

José I. Morell,[a] Demetre J. Economou,[b] and Neal R. Amundson
Department of Chemical Engineering, University of Houston, Houston, Texas 77204-4792

(Received 25 August 1992; accepted 29 December 1992)

A mathematical model was developed to elucidate the interaction between transport/reaction processes and the evolution of porosity in chemical vapor infiltration with microwave heating (MCVI). The analysis included a set of partial differential equations describing the spatiotemporal variation of gaseous species concentration, composite temperature, porosity, and stress. Maxwell's equations were used to determine the distribution of power dissipated inside the composite. The deposition of silicon carbide was selected as a model chemical system to explore the general features of MCVI. MCVI can provide a favorable temperature distribution in the composite yielding an inside-out deposition pattern, thereby preventing entrapment of accessible porosity. For this temperature profile, tensile stresses develop at the outer regions and compressive stresses are found in the composite core. For a given system there exists a minimum value of the coefficient for heat transfer from the composite surface, h, below which accessible porosity is trapped within the composite. Similarly, there exists a maximum value of the incident microwave energy flux, I_0, above which accessible porosity is trapped within the composite. I_0 and h can be optimized for a given preform to achieve complete densification with minimum processing time. Using the technique of pulsed-power, the processing time can be reduced even further without compromising density uniformity. Power dissipation profiles in the composite depend strongly on preform thickness, microwave frequency, and relative loss factor.

I. INTRODUCTION

Chemical vapor infiltration (CVI) is considered one of the leading techniques for the fabrication of fiber-reinforced ceramic composites.[1,2] Interest in these composites stems from their superior fracture toughness, reliability, durability, and noncatastrophic failure which make them attractive for a wide range of high-temperature applications.[3] In CVI, gaseous reactants infiltrate a heated porous preform and decompose to deposit a solid matrix, thereby filling the pores.[4] Important goals of VCI include uniform densification and short processing time.

In traditional CVI, densification is achieved by heating the preform to the appropriate temperature in a furnace. In this isothermal CVI method, reactants are depleted as they diffuse from the surface of the composite inward. Reactant depletion causes preferential deposition close to the surface, and the eventual sealing of the external transport conduits. The final result is significant porosity entrapment within the composite. In order to minimize reactant depletion, one has to use a low processing temperature. Such action, however, leads to long processing times which can reach several weeks. Several alternative methods have been proposed to overcome some of the limitations of the isothermal process. These include pressure-driven, temperature-gradient, and pulsed-pressure CVI.

An emerging technique that may prove superior to other CVI methods uses microwave heating. Advantages of this technique include rapid and selective heating, fast response to changes in power, and the potential to produce ceramics with particular microstructural properties.[5,6] So far, microwave heating has been applied mainly to sintering, but it appears to be promising for CVI as well. The distinct feature of CVI with microwave heating is that absorption of power is achieved throughout the volume of the composite. This leads to a temperature that increases monotonically from the composite surface toward the center. Since the deposition rate is usually a monotonic function of both reactant concentration and temperature, reactant depletion is counterbalanced by the increasing temperature as the gases diffuse toward the composite center. In fact, judicious selection of the microwave power can lead to an inside-out densification of the composite without residual accessible porosity.

Mathematical models provide a basis for understanding the complex interaction of transport and reaction processes taking place in CVI. Model predictions can suggest process improvements, novel reactor configurations, and better process control strategies. There have been several theoretical studies of CVI and some

[a]Present address: Shell Development Co., Bellaire Research Center, P.O. Box 481, Houston, Texas 77001.
[b]Author to whom correspondence should be addressed.

examples are given next. A pressure-driven, temperature-gradient CVI was investigated by Tai and Chou[7] using a two-dimensional model for the deposition of SiC. Based on a model for forced-flow CVI, Gupte and Tsamopoulos[8] concluded that forced flow of reactants can improve the uniformity of densification. Middleman[9] and Sheldon[10] showed that proper selection of the system chemistry may lead to process improvements. Melkote and Jensen[11] used Monte Carlo simulations to describe the evolution of the structural parameters of the composite. They studied the effect of temperature under isothermal and temperature-gradient conditions. Pulsed-pressure CVI was studied by Sotirchos,[12] employing a model to describe the dynamic behavior of the process.

Mathematical modeling can be especially useful for as yet undeveloped processes such as CVI with microwave heating. The first study of CVI with microwave heating was reported by Gupta and Evans.[13] These authors used a very simplified model of the preform structure (a single pore model) and pseudosteady-state equations to describe the processing of a SiC composite. Shortly thereafter, a mathematical model of CVI with volume heating was proposed by Morell *et al.*[14] In this investigation, a detailed description of the transport-reaction processes and of the evolving pore structure was included. Model results revealed the existence of a critical value of power density above which entrapment of otherwise accessible porosity occurs. In a follow-up study, Morell *et al.*[15] proposed a novel technique called pulsed-power volume-heating CVI. In this technique the power of the volume-heating source (e.g., microwaves) is modulated according to a prescribed wave form. A window of operating conditions was identified leading to substantial improvements in deposit uniformity with simultaneous reduction in processing time (as compared to cw operation). These studies, however, assumed thin samples and, hence, microwave power attenuation was not considered. Furthermore, the possibility of excessive stress development in the composite was not examined.

The present study is an extension of our previous works. A mathematical model is developed to elucidate the interaction between transport/reaction processes and the evolution of the porous matrix in microwave chemical vapor infiltration (MCVI). The analysis includes a set of equations describing the space and time dependence of species concentration, temperature, pressure, porosity, and stress distribution. In addition, Maxwell's equations are used to determine the distribution of power dissipated inside the composite. The deposition of silicon carbide in a silicon carbide fiber preform is selected as a model chemical system to explore the general features of MCVI.

Results show that MCVI can result in a favorable temperature profile (with temperature increasing monotonically toward the composite center) that leads to an inside-out densification pattern. For this temperature profile, tensile stresses develop at the surface, whereas compressive stresses are found at the composite core. In some regions of the parameter space, a standing wave of dissipated power is established that can affect the temperature distribution in the composite. Power pulsing can provide a window of operating conditions for achieving significant improvement in deposit uniformity as well as reduction in processing time.

II. DEVELOPMENT OF THE MATHEMATICAL MODEL

The system being investigated consists of a free-standing preform of slab geometry and width $2L$ as shown in Fig. 1. The preform length and height are assumed to be much larger than its width so that a one-dimensional analysis is applicable. The preform is composed of cylindrical fibers oriented randomly in three-dimensional space and resides in an appropriate microwave cavity. Microwaves are incident symmetrically onto both faces of the preform with the same uniform power per unit surface area (P_z). Gaseous precursors of known composition and temperature flow continuously through the cavity keeping a constant species composition at the preform surface. Gaseous reactants infiltrate the preform and decompose to deposit a solid. Deposition continues until complete densification is achieved. The goal is to calculate the spatial and temporal variations in temperature, pressure, reactant and product species concentration, and microwave power dissipation, stress, and porosity. Ultimately one is interested in the final density and mechanical properties of the composite and the total densification time.

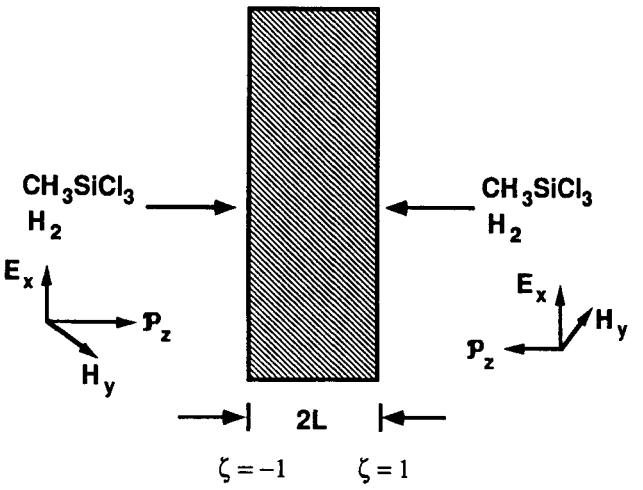

FIG. 1. Schematic of the CVI system with microwave heating. A slab is heated symmetrically by microwaves traveling in the z-direction. The electric and magnetic field vectors are also shown.

A. Microwave heating

To determine the power dissipated in the composite, Φ, we consider the propagation of plane waves in the z-direction incident symmetrically and normal to the sides of the composite located at $z = \pm L$ (Fig. 1). The local electric field is found from Maxwell's equations, which for the system of interest reduce into a single phasor expression as follows[16]

$$\nabla^2 \mathbf{E}_s - \gamma^2 \mathbf{E}_s = 0 \tag{1}$$

in which $\mathbf{E}_s$ is the spatially dependent electric field. Quantity γ is known as the complex propagation constant and is given by

$$\gamma = \omega\sqrt{\mu_0\epsilon_0(-k' + \mathbf{i}k'')} = \alpha + \mathbf{i}\beta \tag{2}$$

where the attenuation and phase factors are given by Eqs. (3) and (4), respectively:

$$\alpha = \omega\sqrt{\mu_0\epsilon_0}\sqrt{\frac{k'\left(\sqrt{1 + (k''/k')^2} - 1\right)}{2}} \tag{3}$$

$$\beta = \omega\sqrt{\mu_0\epsilon_0}\sqrt{\frac{k'\left(\sqrt{1 + (k''/k')^2} + 1\right)}{2}} \tag{4}$$

In the above equations, $\omega(= 2\pi f)$ is the angular frequency of the applied field, $k'(= \epsilon'/\epsilon_0)$ is the relative dielectric constant, and $k''(= \epsilon''/\epsilon_0 = \sigma_c\omega^{-1}/\epsilon_0)$ is the relative loss factor. The relative dielectric constant accounts for the polarization of a medium caused by an applied electric field. The relative loss factor accounts for the development of currents that lead to the thermal dissipation of energy.

Invoking appropriate continuity conditions at the interfaces between ceramic and surrounding medium (assumed to be free space), one can obtain the following expression for the electric field, E_x:

$$E_x = 2\eta_c E_0 e^{L(\gamma_0 - \gamma_c)} \frac{(e^{-\gamma_c z} + e^{\gamma_c z})}{[(\eta_0 + \eta_c) - (\eta_0 - \eta_c)e^{-2\gamma_c L}]}, \quad -L \leq z \leq L \tag{5}$$

where E_0 is the amplitude of the incident wave, subscripts zero and c denote free-space and ceramic properties, respectively. The intrinsic impedance of medium m can be obtained from

$$\eta_m = \sqrt{\frac{\mu_0}{\epsilon_0(k_m' - ik_m'')}} \tag{6}$$

The power dissipated per unit volume of composite can then be obtained from

$$\Phi = \frac{1}{2}\omega\epsilon_0 k''(E_x \cdot E_x^*) \tag{7}$$

For thin samples, Eq. (5) yields a constant value of the electric field strength in the ceramic, implying that attenuation of the microwave field is negligible. This assumption was made in previous analyses of MCVI.[14,15] In Eq. (7) the relative loss factor k'' is a function of porosity, and perhaps more importantly, it is a function of temperature (normally k'' increases with temperature). If k'' depends strongly on temperature, microwave heating may be problematic. As the ceramic absorbs energy and its temperature increases, the loss factor k'' increases as well, and even more energy is absorbed. This feedback mechanism can lead to thermal runaway.[17] The simplest form of porosity dependence is

$$k'' = (1 - \phi)k_c'' + \phi k_0'' \tag{8}$$

where ϕ is the total porosity. The electric field strength of the incident wave may also be written in terms of the incident energy flux using the following relation

$$I_0 = \frac{1}{2}\sqrt{\frac{\epsilon_0}{\mu_0}}E_0^2 \tag{9}$$

B. Thermal stresses and heat transport

During CVI the ceramic composite is subjected to high temperatures that may lead to the development of significant thermal stresses. In general, thermal stresses may be induced by a nonuniform temperature variation within the medium, differences in thermomechanical properties in a multicomponent medium, or by directional variations in the properties of the material. In this study our purpose is to assess the thermal stresses due to temperature gradients to assure that crack initiation does not occur.

To evaluate the stress distribution we consider that the thickness of the slab is small compared to the lateral dimensions, the slab faces are free of tractions, and that the system is symmetric about the midplane. This leads to a plane stress problem,[18] i.e.,

$$\sigma_{zz} = \sigma_{zy} = \sigma_{zx} = \sigma_{xy} = 0 \tag{10}$$

The stresses can then be readily found from the compatibility conditions

$$\sigma_{xx} = \sigma_{yy} = \sigma = \frac{\alpha_T E}{1 - \nu}\left[\frac{1}{L}\int_0^L T(t,z)\,dz - T(t,z)\right] \tag{11}$$

whereas the strains are obtained from the stress-strain relations

$$\epsilon_{xx} = \epsilon_{yy} = \alpha_T\left[\frac{1}{L}\int_0^L T(t,z)\,dz - T_0\right] \tag{12}$$

$$\epsilon_{zz} = \frac{\alpha_T}{1-\nu} \cdot \left[-\frac{2\nu}{L}\int_0^L T(t,z)\,dz + (1+\nu)T(t,z) - (1-\nu)T_0 \right] \quad (13)$$

$$\epsilon_{zy} = \epsilon_{zx} = \epsilon_{xy} = 0 \quad (14)$$

The thermomechanical properties are the coefficient of thermal expansion, α_T, Young's modulus of elasticity, E, and Poisson's ratio, ν. These properties are assumed to be constant. It should be noted that the thermal stress problem can be solved independently from the temperature distribution. This is because the thermoelastic dissipation term in the energy balance is negligible. In Eqs. (12) and (13), T_0 is a base temperature at which the strains in the material are zero (here taken as 300 K). We realize that the above equations apply to a homogeneous isotropic medium. However, we still use these equations to obtain an order of magnitude estimate of the stresses in the composite.

Temperature variations inside the composite are described by

$$C_p^e \frac{\partial T}{\partial t} - \nabla\cdot(k^e \nabla T) + \sum_{r=1}^{n^G}(\mathbf{N}_r C_{p_r}) \cdot \nabla T + \sum_{i=1}^{n^R}(\Delta H_i R_i) = \Phi, \quad (15)$$

where C_p^e and k^e are the effective heat capacity per unit volume and effective thermal conductivity of the fiber-matrix composite, respectively. The first term on the left-hand side of Eq. (15) is an energy accumulation term, whereas the second to fourth terms account for heat conduction, convection, and heat of reaction, respectively. The term on the right-hand side represents the power dissipated per unit volume of composite [Eq. (7)] due to microwave heating.

C. Mass transport and chemical reaction

The conservation equation for the rth gaseous species is given by

$$\phi_A C\frac{\partial x_r}{\partial t} + \nabla\cdot\mathbf{J}_r + \mathbf{N}\cdot\nabla x_r = \sum_{i=1}^{n^R}\upsilon_{ri}R_i - x_r\sum_{r=1}^{n^G}\sum_{i=1}^{n^R}\upsilon_{ri}R_i \quad (16)$$

where ϕ_A is the accessible porosity, C is the total gaseous concentration, and x_r and $\mathbf{J}_r$ are the mole fraction and the diffusive flux of the rth species, respectively. $\mathbf{N}$ is the total molar flux, n^G and n^R are the number of gaseous species and chemical reactions considered in the model, and R_i is the rate of the ith reaction per unit volume of composite.

The molar fluxes for a mixture of three gaseous species, as the one considered in this study, are obtained from the Dusty Gas model assuming negligible contributions to the fluxes by surface diffusion, thermal diffusion, and thermal transpiration,[19]

$$J_1 = -\Delta_{12}\Delta_{23}\Delta_{31} \cdot \frac{\{A_1/\Delta_{23} - x_1[A_1(1/\Delta_{23} - 1/\Delta_{12}) + A_2(1/\Delta_{31} - 1/\Delta_{12})]\}}{[x_1(\Delta_{23} - \Delta_{12}) + x_2(\Delta_{31} - \Delta_{12}) + \Delta_{12}]} \quad (17)$$

$$J_2 = -\Delta_{12}\Delta_{23}\Delta_{31} \cdot \frac{\{A_2/\Delta_{31} - x_2[A_1(1/\Delta_{23} - 1/\Delta_{12}) + A_2(1/\Delta_{31} - 1/\Delta_{12})]\}}{[x_1(\Delta_{23} - \Delta_{12}) + x_2(\Delta_{31} - \Delta_{12}) + \Delta_{12}]} \quad (18)$$

where

$$A_r = \frac{P}{RT}\nabla x_r + \frac{x_r}{RT}\left(1 - \frac{1}{D_r^e\sum_{s=1}^{n^G} x_s/D_s^e}\right)\nabla P \quad (19)$$

$$\frac{1}{\Delta_{rs}} = \frac{1}{D_{rs}^e} + \frac{1}{D_r^e D_s^e\sum_{t=1}^{n^G} x_t/D_t^e} \quad (20)$$

The previous equations in conjunction with the constraint that the sum of the diffusive molar fluxes must be zero and a corresponding equation for the total flux constitute a complete set of independent equations for the molar fluxes.

The spatiotemporal dependence of the accessible porosity can be obtained from the following equation

$$\frac{\partial\phi_A}{\partial t} = -\frac{M_s}{\rho_s}\sum_{i=1}^{n^R} V_{ki}R_i \quad (21)$$

in which M_s and ρ_s are the molecular weight and density of the deposited solid, respectively. The rate of ith reaction per unit volume of composite, R_i, is given by

$$R_i = \begin{cases} \phi_A R_i^*; & \text{for a homogeneous reaction} \\ S_A R_{si}; & \text{for a heterogeneous reaction} \end{cases} \quad (22)$$

where R_i^* is the reaction rate per unit volume of gas, R_{si} is the reaction rate per unit surface area, and S_A is the accessible surface area per unit volume of composite.

In order to characterize the process, the average trapped accessible porosity, $\overline{\phi}_{A,T}$, is introduced as a measure of deposit nonuniformities. This is given by

$$\frac{\overline{\phi}_{A,T}}{\phi_{A,0}} = \frac{1}{L}\int_0^L\left(\frac{\phi_{A,T}}{\phi_{A,0}}\right)dz \quad (23)$$

where $\phi_{A,T}$ represents trapped porosity that can no longer be infiltrated by the reactant. Such a situation occurs, for example, when premature sealing of the pores near the preform surface does not allow reactant to penetrate deeper into the preform, resulting in trapped porosity.

The governing equations are subject to the following boundary and initial conditions:

$$\text{at } z = 0 \quad \nabla x_r = 0, \quad \nabla P = 0, \quad \nabla T = 0 \tag{24}$$

$$\text{at } z = L \quad x_r = x_{rb}, \quad P = P_b, \quad -k^e \nabla T = h(T - T_b) + \sigma_{SB}\bar{\epsilon}(T^4 - T_b^4) \tag{25}$$

$$\text{at } t = 0 \quad x_r = x_{r0}, \quad P = P_0, \quad T = T_0, \quad \phi_A = \phi_{A,0} \tag{26}$$

D. Preform structure and model parameters

The transport properties of the multicomponent gaseous mixture were determined using the Chapman–Enskog theory.[20] The mathematical formulation accounts for the dependence of these properties on temperature, pressure, composition, and structural changes of the composite. Thermodynamic properties also account for temperature variations as well as the two-phase nature of the system. The variation of the structural parameters of the preform can be found in the literature.[14,21,22]

E. Chemical kinetics

In the present study we considered the deposition of silicon carbide from the decomposition of methyltrichlorosilane (MTS) as a model chemical system. Although this system has been the subject of several investigations, there still exists considerable uncertainty about the reaction mechanism and kinetic parameters.[23–25] Since our main emphasis was on microwave heating, simplified chemical kinetics was used, whereby the deposition of SiC was described by the following overall reaction

$$CH_3SiCl_3 \longrightarrow SiC + 3HCl \tag{27}$$

The deposition rate is then given by

$$R_{sl} = x_{MTS} C k_1 \exp[-E_1/(RT)] \tag{28}$$

where the pre-exponential factor and activation energy are $k_1 = 2.62$ m/s and $E_1 = 120$ kJ/mol, respectively.[25] In accordance with Eq. (27), three gaseous components are included in the model, namely, methyltrichlorosilane, hydrogen chloride, and hydrogen (an inert). Equation (28) does not include possible etching of SiC by the HCl by-product. More complicated deposition/etching kinetics could be readily included in the model except that kinetic information is unavailable.

F. Numerical method

The method of lines was used to solve the set of partial differential equations describing the behavior of the system. The discretization of the spatial derivatives was accomplished using orthogonal collocation on finite elements with B-splines basis functions.[26] The number of collocation points was chosen such that the spatial and temporal variations of the power dissipated within the composite could be captured. The resulting set of ordinary differential equations was integrated in time using a variable-step variable-formula method. The CPU time needed to obtain the solution varied from 1 to 15 min of CRAY-YMP, depending on the parameter values used.

III. RESULTS AND DISCUSSION

The behavior of MCVI is elucidated by studying the response of the system to changes of several key parameters. A SiC preform with an initial accessible porosity of 0.5 is considered. The initial temperature of the preform and the ambient temperature is 300 K. Physical and transport properties of the gaseous species and preform properties are given in Table I. Basic parameter values used for calculations are shown in Table II. Parametric studies were carried out by varying the value of one parameter while keeping the other parameters constant. The basic parameter values were used unless stated otherwise.

The power dissipated per unit volume within the composite Φ is an important quantity that dictates the temperature distribution and, hence, the time evolution of densification. The spatial dependence of Φ on the half-thickness of the preform is shown in Fig. 2. For small values of L (e.g., 1 mm) the power decreases

TABLE I. Physical and transport properties.

$D_1^e = 3.96\frac{\phi}{\eta_M} d_p T^{0.5}, \text{m}^2/\text{s}$	$D_2^e = 8.03\frac{\phi}{\eta_M} d_p T^{0.5}, \text{m}^2/\text{s}$
$D_3^e = 34.16\frac{\phi}{\eta_M} d_p T^{0.5}, \text{m}^2/\text{s}$	$D_{12} = 1.57 \times 10^{-9}\ T^{1.5}/(P\Omega_{12}), \text{m}^2/\text{s}$
$D_{13} = 6.75 \times 10^{-9}\ T^{1.5}/(P\Omega_{13}), \text{m}^2/\text{s}$	$D_{23} = 1.42 \times 10^{-8}\ T^{1.5}/(P\Omega_{23}), \text{m}^2/\text{s}$
$M_1 = 149.48$ g/mol	$M_2 = 36.46$ g/mol
$M_3 = 2.01$ g/mol	$\rho_c = 3.21$ g/cm^3

TABLE II. Basic parameter values used for calculations.

Symbol	Name	Basic value
L	Half preform thickness	1 mm
$\phi_{A,0}$	Initial accessible porosity	0.5
h	Heat-transfer coefficient	329 W/(m^2 K)
P_0	Initial pressure	1 atm
r_f	Fiber radius	4.0 μm
T_b	Ambient temperature	300 K
T^r	Reference temperature	1000 K
x_{1b}	CH_3SiCl_3 mole fraction	0.1
x_{2b}	Hydrogen mole fraction	0.9
I_0	Incident energy flux	1.5 MW/m^2
f	Frequency	2.45 GHz
k'	Relative dielectric constant	60
k''	Relative loss factor	35
k	Thermal conductivity of SiC	10 J/(m s K)
k^r	Reference thermal conductivity	6.58×10^{-2} J/(m s K)
E	Young's modulus of elasticity	400 GPa
ν	Poisson's ratio	0.2
α_T	Coefficient of thermal expansion	5.0×10^{-6} K^{-1}

monotonically from the center (dimensionless distance $\zeta = 0$) toward the surface of the composite (dimensionless distance $\zeta = 1$). Such spatial variations of power arise when the ratio of the wavelength of the microwaves to composite half-thickness λ_p/L is greater than unity. In fact, for very small values of L the power density is nearly constant. An increase in L, however, leads to a wave pattern of power deposition. This happens when the wavelength to half-thickness ratio λ_p/L is about unity or smaller. When L is very large there results an almost exponential decay of dissipated power.

Figure 3 illustrates the dimensionless power dissipation as a function of position for several values of the loss factor k''. The dimensionless power is defined as $\Phi^* = \Phi L^2/(T^r k^r)$, where T^r and k^r are reference values for temperature and thermal conductivity (Table II). A wave-like profile is obtained, and power dissipation increases with k''. At present, data on the variation of k'' with temperature and frequency are scanty. Such data are important if more precise predictions are to be made.

Figure 4 shows that the spatial power dissipation profiles depend strongly on frequency. Conditions were as in Fig. 3 except that f was set at 31 GHz. The 3-D plot illustrates that a wave pattern emerges for a loss factor less than about 12. Larger values of k'' lead to significant attenuation of the microwaves, and Φ becomes essentially zero in the inner core of the composite (near $\zeta = 0$). In general, the power dissipation profiles are described by a combination of exponential and sine-like factors [see Eq. (5)]. The exponential factors predominate for large values of k''. The power dissipation profiles affect the temperature distribution in the composite. When the thermal conductivity of the composite is low, a wave-like temperature distribution is obtained following the power dissipation profile. However, for high values of the thermal conductivity, nonuniformities in power dissipation are smoothed out.

We now turn to the densification process. It is useful to consider some results of the isothermal CVI first since they can provide a basis for comparison. It was found that at a temperature of 1000 K one can obtain excellent density uniformity at the expense of long processing time (≈40 h). On the other hand, temperatures higher than 1300 K resulted in preferential deposition close to

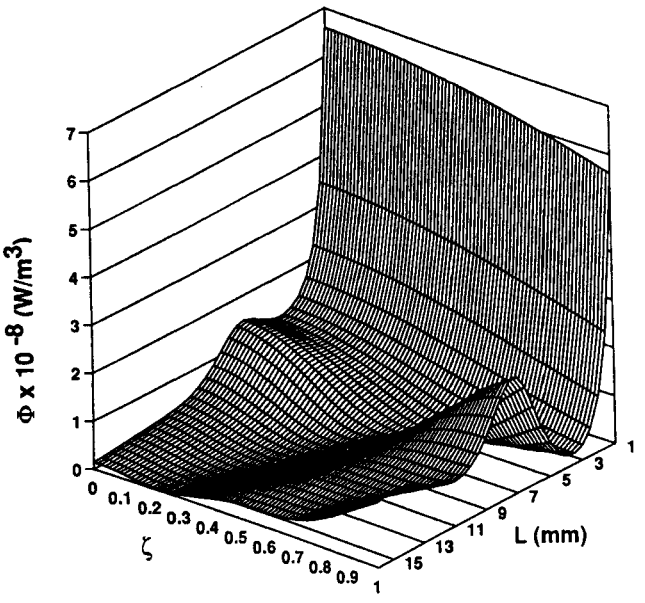

FIG. 2. Power dissipation as a function of distance within the composite for different half-thicknesses L. Other parameters at their basic value.

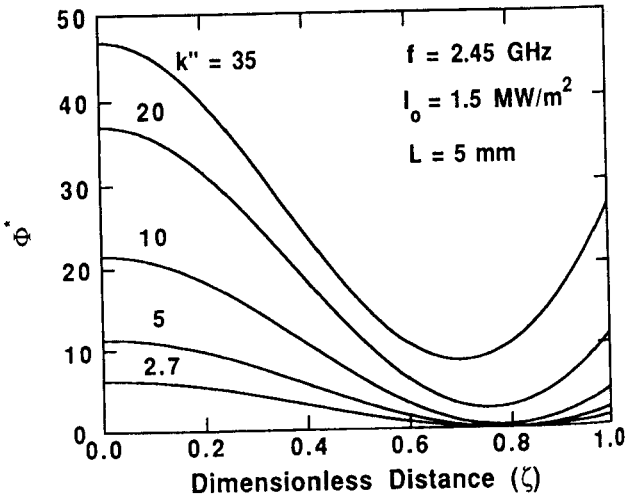

FIG. 3. Power dissipation as a function of distance within the composite for several values of the relative loss factor k''. Other parameters at their basic value.

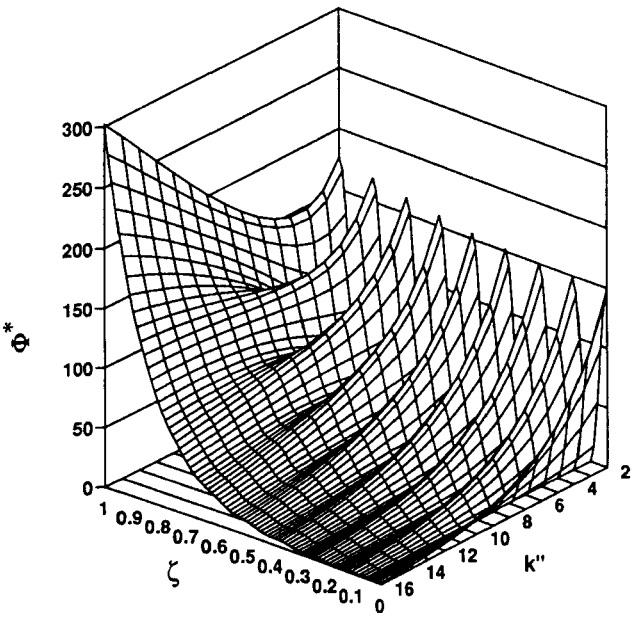

FIG. 4. Power dissipation as a function of distance within the composite for several values of the relative loss factor k''. Other parameters at their basic value except that $f = 31$ GHz and $L = 5$ mm.

the surface of the composite and eventual closure of the surface pores. Hence, isothermal CVI is constrained to low operating temperatures.

Figure 5 shows the spatiotemporal variation of the reduced accessible porosity for MCVI and for the basic parameter values. Under these conditions, microwave heating leads to almost constant porosity profiles at the initial stages of the process. At later times, however, the porosity is lower at the center and higher at the surface of the composite; i.e., an inside-out deposition pattern is obtained. A lower processing time is also obtained, as compared to isothermal conditions. The underlying factor responsible for this behavior is the spatial variation of the composite temperature, shown in Fig. 6. The temperature exhibits a maximum at the center and decreases monotonically toward the surface of the composite. Such a temperature profile allows for a deeper infiltration of reactant within the composite and prevents the early closure of the surface pores. Similar findings were reported for volume-heating CVI of carbon, as well as pulsed-power volume-heating CVI.[14,15] It should be noted that the temperature gradients prevailing within the fiber-matrix composite depend significantly on the effective thermal conductivity and its evolution during the deposition process. In addition, surface cooling of the composite is necessary in order to achieve enough temperature gradient for inside-out densification to occur. This is in contrast to microwave sintering in which the sample is insulated. Surface cooling can be achieved by radiation to the cooled microwave cavity walls and forced gas flow over the sample.

The spatially averaged trapped accessible porosity and processing time as a function of the heat-transfer coefficient are shown in Fig. 7. Trapped accessible porosity refers to the porosity that otherwise would have been accessible to the reactants but has been trapped because of premature pore sealing. The processing time $\tau_{10\%}$ is the time needed for the composite to reach an average accessible porosity of 10% of its initial value ($\overline{\phi}_A/\phi_{A0} = 0.1$). Increasing the heat-transfer coefficient leads to a substantial reduction in the trapped accessible porosity. Actually, there exists a minimum value of h above which no entrapment of porosity occurs. However, as h increases, the time required for complete densification increases as well. It appears that $h \sim 330$ W/m^2-K is near optimum for the conditions examined. A similar behavior (not shown) is obtained when the incident power flux, I_0, is the varying parameter. Increasing I_0

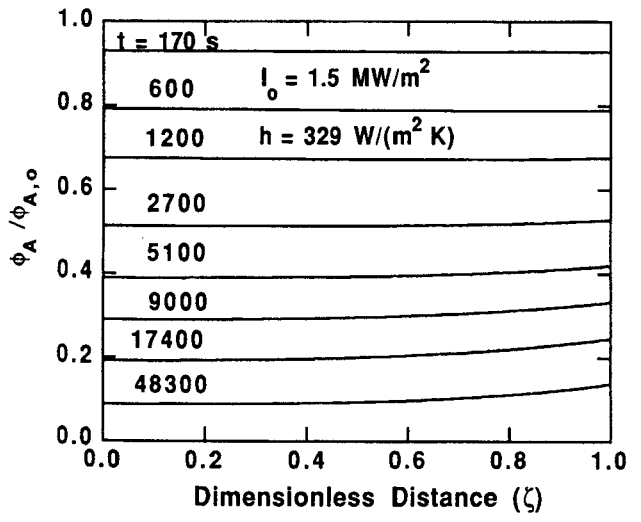

FIG. 5. Time evolution of accessible porosity profiles. Parameters at their basic value.

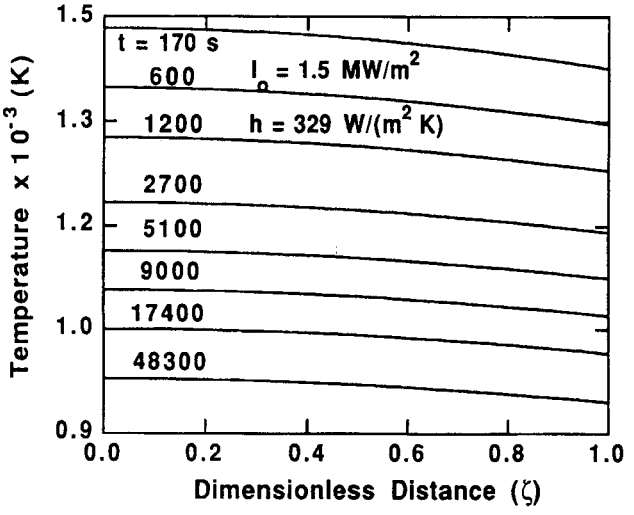

FIG. 6. Time evolution of temperature profiles. Parameters at their basic value.

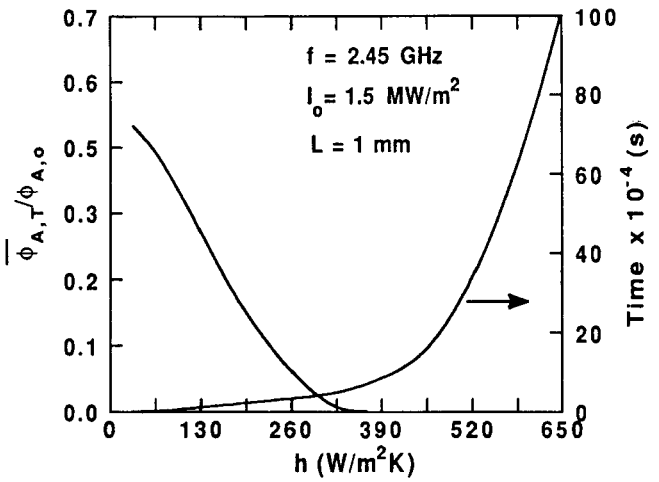

FIG. 7. Variation of the spatially averaged trapped porosity and of processing time with the heat-transfer coefficient. Other parameters at their basic value.

reduces $\tau_{10\%}$, but values of I_0 exceeding 1.6 MW/m^2 would result in the development of trapped accessible porosity. The relative loss factor also affects the variation of $\overline{\phi}_{AT}/\phi_{A0}$, particularly as the preform size is increased. When a 1 cm-thick preform (L = 5 mm) is used, k'' values larger than seven would result in an early sealing of the surface pores, and, hence, a large portion of the preform would remain undensified.

The stress profiles ($\sigma = \sigma_{xx} = \sigma_{yy}$ in dimensionless units) as a function of time are shown in Fig. 8 for the basic parameter values. One can see the development of tensile stresses extending from a dimensionless position of about 0.6 toward the surface, whereas compressive stresses develop in the remainder of the composite. The temperature distribution is accountable for this behavior, since temperatures below the average lead to tensile stress and above the average result in compressive stress. Tensile stresses are larger than compressive stresses reaching a maximum value of 0.04 dimensionless units located at the surface. At this point some comments are in order regarding possible crack initiation and fracture. It is reasonable to assume that the initial fracture behavior of the composite is determined primarily by the tensile strength of the fibers. A typical value for the tensile strength of SiC fibers is 900 MPa. This value corresponds to a critical dimensionless stress of 0.36 units. Since the critical stress is significantly larger than 0.04, no crack initiation is expected for these conditions. It is important to note that when the loss factor k'' increases sharply with temperature, the likelihood of obtaining crack initiation due to thermal stresses is very high. In fact, complete meltdown of the ceramic may occur in such cases due to thermal runaway. Special power modulation schemes can be used to circumvent these problems.[17]

The corresponding strain profiles in the zz-direction as a function of time are illustrated in Fig. 9. These profiles exhibit a spatial dependence similar to that of the composite temperature (Fig. 6). The maximum strain is about 0.61% and occurs at the center of the composite. The strain increases sharply with time at early times and decreases thereafter, following the behavior of the composite temperature. At later times the effective thermal conductivity and heat capacity of the composite increase because of densification, leading to lower temperatures. The strains in the xx- and yy-directions are spatially independent.

To evaluate the impact of power dissipation profiles on MCVI, Fig. 10 shows the spatiotemporal variations of the stress for a 10 mm-thick preform and for f =

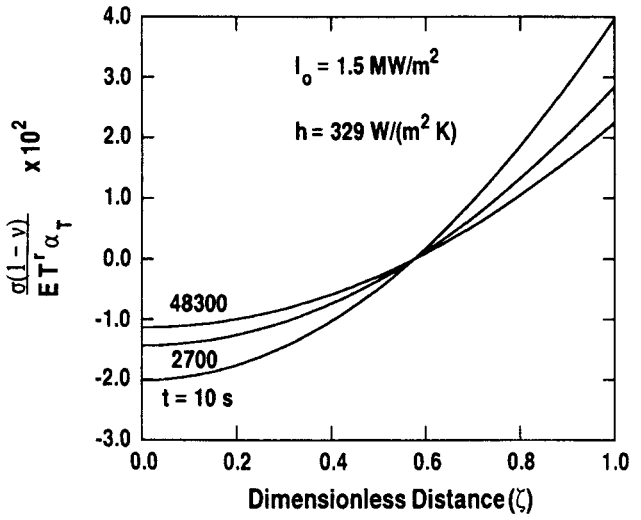

FIG. 8. Time evolution of stress profiles. Parameters at their basic value.

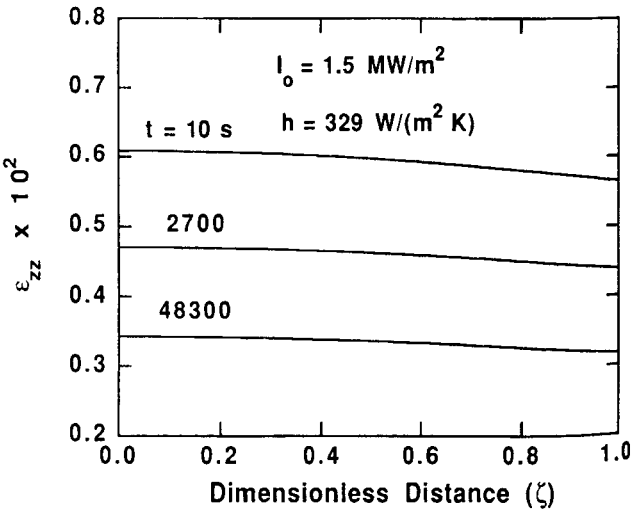

FIG. 9. Time evolution of strain profiles in the zz-direction. Parameters at their basic value.

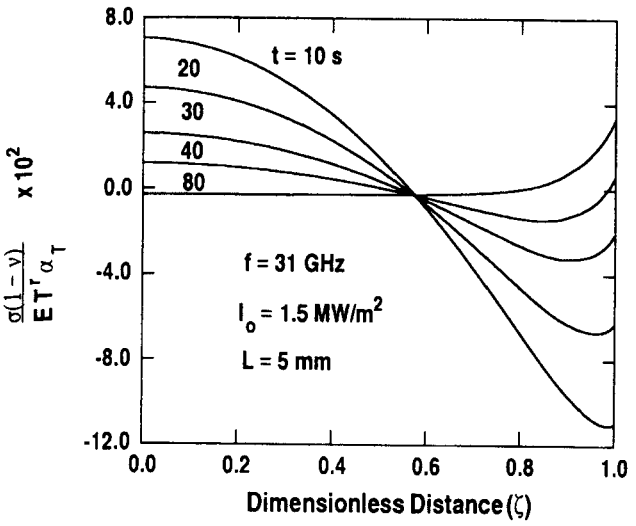

FIG. 10. Time evolution of stress profiles. Parameters at their basic value except that $f = 31$ GHz and $L = 5$ mm.

31 GHz. Under these conditions Φ decreases exponentially toward the center of the composite, resulting (initially) at higher surface temperature. This is the opposite temperature distribution from that desired for successful MCVI. The stress profile shows tensile stresses in the core region and compressive stresses in the remainder of the composite. At later times, however, the surface temperature diminishes (not shown) due to the heat dissipation from the composite surface by convection and radiation. During that time, the center temperature increases and eventually becomes higher than the surface temperature. Consequently, the surface stress changes from a compressive stress of 0.11 dimensionless units to a tensile stress of 0.03 units in a period of less than 70 s. During the same period, the center stress varies from 0.07 to −0.01 units. It should be noted that, although the temperature eventually attains a minimum at the surface, these operating conditions will lead to early closure of the surface pores and entrapment of porosity in the composite core.

Pulsed-power MCVI

Microwave CVI with pulsed-power has been found to provide substantial reductions in processing time without compromising density uniformity.[15] In this technique, the source power is modulated in time with a specific period and duty cycle. During the low-power part of the cycle, the temperature of the composite decreases, reducing the reaction rate and thus allowing the reactants to diffuse into the composite. This alleviates diffusional limitations within the composite, minimizing density nonuniformities. The high-power part of the cycle leads to rapid reaction rates, thereby minimizing the processing time. Pulsed-power simulations showed, for example, that the entrapment of porosity that develops for the case with $I_0 = 1.7$ MW/m^2 (other parameters as shown in Table II) is completely avoided with a 20% reduction in processing time.

IV. SUMMARY AND CONCLUSIONS

The transport, reaction, and thermoelastic phenomena taking place in microwave chemical vapor infiltration have been investigated using a mathematical model. A preform of slab geometry consisting of randomly oriented SiC fibers was studied. MTS in a H_2 carrier gas was used as the precursor for the deposition of the SiC matrix. The model included partial differential equations to describe the spatial and temporal variations of the gaseous species composition, composite temperature, porosity, and stress. Maxwell's equations provided the power dissipated in the composite as a function of several key parameters including preform thickness, loss factor, and frequency of microwave field.

Model results showed that MCVI can provide a favorable temperature profile in the composite with temperature increasing from the surface to the center of the composite. This profile yields an inside-out deposition pattern, thereby preventing entrapment of accessible porosity. In addition this temperature profile leads to tensile stresses at the outer regions and compressive stresses at the core of the composite. However, the opposite stress profile can develop at early times although this lasts for a very short time. These phenomena are more pronounced for high frequency and/or large loss factor k''. For a given preform there exists a minimum heat-transfer coefficient below which accessible porosity is trapped within the composite. This underscores the need to cool the composite surface in order to obtain a favorable temperature distribution. Similarly, there exists a maximum I_0 above which accessible porosity is trapped within the composite. I_0 and h can be optimized for a given preform to achieve complete densification with minimum processing time. Using the technique of pulsed-power, the processing time can be reduced even further without compromising density uniformity.

Power dissipation profiles depend strongly on preform thickness, microwave frequency, and relative loss factor. For large values of λ_p/L, power dissipation decreases monotonically from the center toward the surface of the composite. Smaller values of λ_p/L result in wave-like power dissipation profiles. For very small values of λ_p/L, power dissipation decreases exponentially from the surface toward the center of the composite. Variations in the composite temperature profiles caused by the spatial dependence of power dissipation were found to depend on the thermal conductivity of the composite. For small values of thermal conductivity, the wave-like power deposition profiles were reproduced in the tem-

perature distribution. On the other hand, for large thermal conductivity the wave-like patterns were smoothed out in the temperature distribution.

In conclusion, a detailed mathematical model of MCVI has been presented, including species transport and reaction, microwave power dissipation, and stress distribution. At the present time accuracy of the model predictions is limited by uncertainties in the deposition kinetics and the lack of information on the dependence of electromagnetic and thermoelastic properties on temperature and microstructure.

LIST OF SYMBOLS

A_r	defined by Eq. (19)
C	gas concentration, kmol/m^3
C_{pr}	heat capacity of the rth gaseous species, kJ/(kmol K)
C_p^e	effective heat capacity of the composite, kJ/(m^3 K)
d_p	average pore diameter, m
D_r	Knudsen diffusion coefficient of the rth gaseous species, m^2/s
D_{rs}	binary diffusion coefficient of the r-s pair, m^2/s
$\mathbf{E}_s$	electric field, V/m
E	Young's modulus of elasticity, Pa
E_i	activation energy of the ith reaction, kJ/kmol
h	heat-transfer coefficient, J/(m^2 s K)
I_0	incident energy flux, W/m^2
$\mathbf{J}_r$	molar flux of the rth species relative to the molar average velocity, kmol/(m^2 s)
k'	relative dielectric constant
k''	relative loss factor
k^e	effective thermal conductivity of the composite, kJ/(m s K)
L	half preform thickness, m
M_r	molecular weight of the rth species, kg/kmol
$\mathbf{N}, \mathbf{N}r$	total molar flux and molar flux of the rth species, respectively, kmol/(m^2 s)
n^G, n^R, n^S	number of gaseous species, reactions, and solid species, respectively
P	pressure, atm
P_z	microwave energy flux, W/m^2
R	gas constant, m^3 atm/(kmol K)
R_i	rate of the ith reaction per unit volume of composite, kmol/(m^3 s)
S_A	accessible surface area per unit volume of composite, m^2/m^3
t	time, s
T	temperature, K
T^r	reference temperature (1000 K)
x_r	mole fraction of the rth species
z	coordinate, m

Greek

α	attenuation constant, m^{-1}
α_T	coefficient of thermal expansion, K^{-1}
β	phase factor, m^{-1}
γ	complex propagation constant, m^{-1}
ΔH_i	heat of the ith reaction, kJ/kmol
Δ_{rs}	defined by Eq. (20), m^2/s
$\epsilon_{xx}, \epsilon_{yy}, \epsilon_{zz}$	strain in the x-, y-, and z-direction
ϵ	dielectric constant, F/m
ϵ_0	dielectric constant of free-space, $(36\pi)^{-1} \times 10^{-9}$ F/m
$\tilde{\epsilon}$	emissivity
ζ	dimensionless distance ($=z/L$)
η	intrinsic impedance, Ω
η_M	tortuosity factor
μ_0	magnetic permeability of free-space, $4\pi \times 10^{-9}$ H/m
ν	Poisson's ratio
ρ_s	density of solid, kg/m^3
σ_c	conductivity, $(\Omega \mathrm{m})^{-1}$
$\sigma_{xx}, \sigma_{yy}, \sigma_{zz}$	stress in the x-, y-, z-direction, Pa
σ_{SB}	Stefan–Boltzmann constant, J/(m^2 s K^4)
$\tau_{10\%}$	processing time, s
υ_{ri}	stoichiometric coefficient for species r in reaction i
$\phi, \phi_A, \phi_{A,T}$	total, accessible, and trapped accessible porosity, respectively
Φ	power dissipation, W/m^3
Φ^*	dimensionless power, $\Phi L^2/(T^r k^r)$
ω	angular frequency ($=2\pi f$), rad/s

Subscripts

0	initial value, free-space value
b	bulk or ambient value
c	composite
$r (r = 1,2,3)$	MTS, HCl, and H_2, respectively
s	solid

Superscripts

e	effective value
r	reference value

ACKNOWLEDGMENT

The authors are grateful to the Pittsburgh Supercomputer Center for making computer time available on the CRAY-YMP Supercomputer.

REFERENCES

1. J.A. Cornie, Y-M. Chiang, D.R. Uhlmann, A. Mortensen, and J.M. Collins, Am. Ceram. Soc. Bull. **65**, 293 (1986).

2. J. R. Strife, J. J. Brennan, and K. M. Prewo, Ceram. Eng. Sci. Proc. **11**, 871 (1990).
3. M. A. Karnitz, D. F. Craig, and S. L. Richlen, Am. Ceram. Soc. Bull. **70**, 430 (1991).
4. T. M. Besmann, R. A. Lowden, B. W. Sheldon, and D. P. Stinton, in *Chemical Vapor Deposition,* edited by K. E. Spear and G. W. Cullen (The Electrochemical Society, Pennington, NJ, 1990), PV **90-12**, p. 482.
5. W. H. Sutton, Am. Ceram. Soc. Bull. **68**, 376 (1989).
6. *Ceramic Transactions 21*, edited by D. E. Clark, F. D. Gac, and W. H. Sutton (American Ceramic Society, Westerville, OH, 1991).
7. N-H. Tai and T-W. Chou, J. Am. Ceram. Soc. **73**, 1489 (1990).
8. S. M. Gupte and J. A. Tsamopoulos, J. Electrochem. Soc. **137**, 3675 (1990).
9. S. Middleman, J. Mater. Res. **4**, 1515 (1989).
10. B. W. Sheldon, J. Mater. Res. **5**, 2729 (1990).
11. R. R. Melkote and K. F. Jensen, in *Chemical Vapor Deposition of Refractory Metals and Ceramics*, edited by T. M. Besmann and B. M. Gallois (Mater. Res. Soc. Symp. Proc. **168**, Pittsburgh, PA, 1990), p. 67.
12. S. V. Sotirchos, AIChE J. **37**, 1365 (1991).
13. D. Gupta and J. W. Evans, J. Mater. Res. **6**, 810 (1991).
14. J. I. Morell, D. J. Economou, and N. R. Amundson, J. Electrochem. Soc. **139**, 328 (1992).
15. J. I. Morell, D. J. Economou, and N. R. Amundson, J. Mater. Res. **7**, 2447 (1992).
16. J. A. Stratton, *Electromagnetic Theory* (McGraw-Hill, New York, 1941).
17. G. A. Kriegsmann, J. Appl. Phys. **71**, 1960 (1992).
18. B. A. Boley and J. H. Weiner, *Theory of Thermal Stresses*, 4th printing (John Wiley, New York, 1967).
19. R. Jackson, *Transport in Porous Catalysts* (Elsevier Publishing Company, New York, 1977).
20. R. B. Bird, W. E. Stewart, and E. N. Lightfoot, *Transport Phenomena* (John Wiley & Sons, New York, 1960).
21. R. R. Melkote and K. F. Jensen, AIChE J. **35**, 1942 (1989).
22. M. M. Tomadakis and S. V. Sotirchos, AIChE J. **37**, 74 (1991).
23. J. Schlichting, Powder Metall. Int. **12**, 141 (1980).
24. F. Langlais, R. Naslain, B. Tarride, and C. Prebende, J. de Physique **50**, 93 (1989).
25. K. Brennfleck, E. Fitzer, G. Schoch, and M. Dietrich, in *Proc. Int. Conf. on CVD*, edited by M. Robison, C. H. J. van den Brekel, G. W. Cullen, J. M. Blocher, Jr., and P. Rai-Choudhury (The Electrochemical Society, Pennington, NJ, 1984), Vol. 84-6, p. 649.
26. C. de Boor, *A Practical Guide to Splines* (Springer-Verlag, New York, 1978).